Bifurcations and chaos in a parametrically damped two-well Duffing oscillator subjected to symmetric periodic pulses

R. Chacón

Departamento de Electrónica e Ingeniería Electromecánica, Escuela de Ingenierías Industriales, Universidad de Extremadura, Apartado Postal 382, E-06071 Badajoz, Spain

A. Martínez García-Hoz

Departamento de Física Aplicada, Escuela Universitaria Politécnica, Universidad de Castilla–La Mancha, E-13400 Almadén (Ciudad Real), Spain

We study a parametrically damped two-well Duffing oscillator, subjected to a periodic string of symmetric pulses. The order-chaos threshold when altering solely the width of the pulses is investigated theoretically through Melnikov analysis. We show analytically and numerically that most of the results appear independent of the particular wave form of the pulses provided that the transmitted impulse is the same. By using this property, the stability boundaries of the stationary solutions are determined to first approximation by means of an elliptic harmonic balance method. Finally, the bifurcation behavior at the stability boundaries is determined numerically. [S1063-651X(99)17105-8]

PACS number(s): 05.45.−a

I. INTRODUCTION

In spite of the complete acceptance of the nonlinear nature of real-world dynamical phenomena, it is still only partially taken into account in the mathematical models, which aim to describe even the simplest of such phenomena. Historically, nonlinearity was first incorporated into low-dimensional dynamical equations in the form of nonlinear potential and dissipative terms. However, for temporal excitations, harmonic functions have been overwhelmingly employed to model them up to now, even though such functions represent solutions of *linear* systems. It has recently been pointed out that it would be more general and appropriate to model temporal excitations by using periodic functions that are solutions of *nonlinear* equations [1]. In the context of second-order differential systems, such as the pendulum and polynomial oscillators [2], the Jacobian elliptic functions (JEF) [3] appear to be the natural candidates fulfilling the requirement of nonlinearity. In comparison with the trigonometric excitations, the JEF's enlarge the parameter space of the system with the elliptic parameter m, that controls the *wave form* of the excitation. In physical terms this means that, having fixed the period, m is responsible for the temporal rate at which energy is transferred from the excitation mechanism to the system. This idea has led to the demonstration of the existence of new generic routes for order↔chaos by changing only the shape of a nonlinear periodic excitation [1]. In this regard, it is a general unresolved problem to characterize the physical conditions under which the aforementioned routes will be independent of the *specific shape* of the excitation, leaving fixed the remaining parameters.

In this present paper we consider some aspects of this broad question in the context of parametrically damped nonlinear oscillators [4–8]. Specifically, we consider the parametrically damped two-well Duffing equation,

$$\frac{d^2x}{dt^2} + \eta[1 + Fp(t;T)]\frac{dx}{dt} - x + x^3 = 0, \quad (1)$$

where η and F are the normalized damping coefficient and the excitation amplitude, respectively, and time is regarded as dimensionless. The function $p(t;T)$ is a generic symmetric pulse of period T and unit amplitude. We first take $p(t;T) \equiv \text{cn}(\omega t;m)$, i.e., the JEF of parameter m. When $m = 0$, then $\text{cn}(\omega t;m=0) = \cos(\omega t)$, i.e., one recovers the previously studied case of harmonic excitation [8]. To investigate the structural stability of the system (1) when only the excitation wave form is varied, we assume that the excitation period T is a frequency-independent parameter, making $\omega = \omega(m) \equiv 4K(m)/T$ with $K(m)$ the complete elliptic integral of the first kind. The parameter space of system (1) is then four-dimensional because of the addition of the parameter m to the three-dimensional parameter space (η, F, T) of the respective harmonic counterpart. Since $\text{cn}(\omega t;m)$ represents a periodic string of symmetric pulses, whose effective width decreases as m increases from $m=0$, in the limiting value $m = 1$ the string vanishes except on a set of instants that has Lebesgue measure zero, i.e., one recovers the autonomous counterpart of Eq. (1). Figure 1(a) shows three plots of the function $\text{cn}[4K(m)t/T;m]$ for different m values. Secondly, we take $p(t;T)$ to be a rectangular-pulse function:

$$s(t;a,T)$$

$$= \left\{ \begin{array}{c} 1, t \epsilon[0,a/2] \cup [T-a/2,T] \\ -1, t \epsilon[T/2-a/2,T/2+a/2] \\ 0 \text{ otherwise,} \end{array} \right\} \text{ in each period } T,$$

$$(2)$$

where a $(a < T/2)$ is the parameter controlling the width of the pulses. The parameters a and m have analogous roles in the two types of pulses. Now, the question is: What would the relationship(s) between a and m (if any) be in order for the dynamics arising from the system (1), solely under changes in the pulse shape, to be the same for both kinds of pulse? In view of the particular form of Eq. (1), a plausible
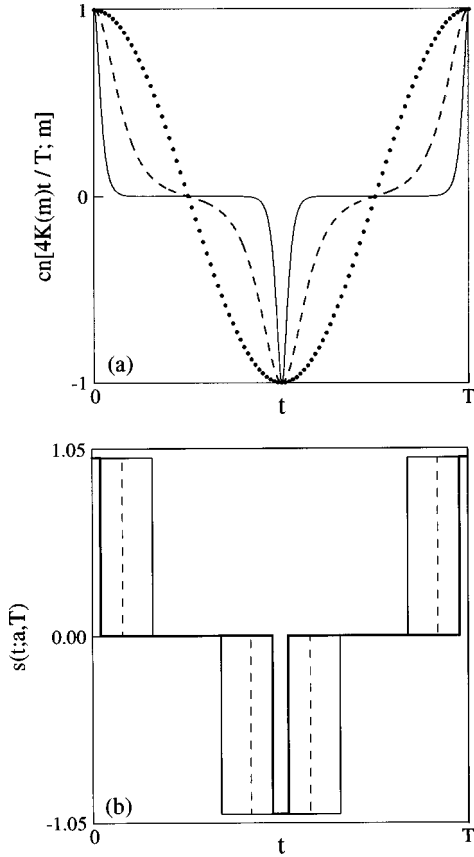
FIG. 1. (a) Pulse function $\mathrm{cn}[4K(m)t/T;m]$ for $T=\mathrm{const}$ and $m=0$ (dotted line), $m=0.999$ (dashed line), and $m=1-10^{-15}$ (solid line). (b) Pulse function $s(t;a,T)$ with $a=a(m,T)$, [cf. Eqs. (2) and (4), respectively], for $T=\mathrm{const}$ and $m=0$ (thin solid line), $m=0.999$ (dashed line), and $m=1-10^{-15}$ (thick solid line). t is a dimensionless variable.

physical condition to derive such a relationship would be to require that the two pulse functions yield the same impulse in the following sense:

$$\int_0^T |\mathrm{cn}(4Kt/T;m)| dt = \int_0^T |s(t;a,T)| dt, \qquad (3)$$

i.e., the proposed relationship reads

$$a=a(m,T) \equiv \frac{T}{2K(m)\sqrt{m}} \arccos(\sqrt{1-m}), \qquad (4)$$

with the limiting values

$$a(m=0,T)=\frac{T}{\pi}, \qquad (5)$$

$$a(m=1,T)=0.$$

Figure 1(b) shows three plots of the driving pulses $s[t;a(m,T),T]$ [cf. Eqs. (2) and (4)] for the same m values as in Fig. 1(a). Of course, one cannot expect that condition (4) be uniformly valid for all the period. Indeed, note that Eq. (1) can be put into the form,

$$\frac{dE}{dt} = -\eta \dot{x}^2(t)[1+Fp(t;T)], \qquad (6)$$

where $E(t) \equiv \frac{1}{2}\dot{x}^2(t) + U[x(t)]$ $[U(x) \equiv -\frac{1}{2}x^2 + \frac{1}{4}x^4]$ is the energy function. Integration of Eq. (6) over *any* interval $[nT,nT+T/4]$, $n=0,1,2,...$, yields

$$E(nT+T/4)-E(nT)=-\eta \int_{nT}^{nT+T/4} \dot{x}^2(t)[1+Fp(t;T)]dt. \qquad (7)$$

Now, given that *all* solutions of Eq. (1) are bounded, the application of the first mean value theorem [14] to the remaining integral in Eq. (7) gives

$$E(nT+T/4)-E(nT)=-\eta \dot{x}^2(t^*)$$
$$\times \left[\frac{T}{4} + F \int_{nT}^{nT+T/4} p(t;T)dt \right], \qquad (8)$$

where $t^* \epsilon [nT,nT+T/4]$. It is clear that, in general, t^* will depend on both n and $p(t;T)$. Since we are interested in asymptotic solutions, consider Eq. (8) for sufficiently large values of n, such that the system is reaching the steady state that corresponds to the given initial condition. Assuming condition (3) holds, one sees that the variation of the energy function, after a quarter period, does not depend on the specific shape of $p(t;T)$ but only on $\dot{x}(t^*)$. Although for symmetric-pulse functions $p(t;T)$ with different wave forms the associated values of $\dot{x}(t^*)$ will not, in general, be the same for large periods $(T \gg 1)$, it would be reasonable to expect the difference to diminish as $T \rightarrow 0$. Thus, the respective dynamics arising from Eq. (1) should be very similar for sufficiently small periods, provided that the remaining parameters and the initial condition are held constant.

The organization of the paper is as follows. In Sec. II we study theoretically the onset of chaos (homoclinic bifurcation) in system (1) through Melnikov analysis (MA) by considering both types of pulse function. The features of the threshold functions in parameter space are discussed, with special emphasis on the shape parameter dependence. Section III gives a preliminary estimate of the stability boundaries for the stationary solutions $(x=\pm 1, \dot{x}=0)$ in parameter space (η,F,T,m). The theoretical approach is based on two assumptions: (a) that the stability boundaries of Eq. (1) can be obtained by analytically solving its linearized equation, and (b) that the truncation of certain generalized Fourier series at lowest order provides an approximate but useful solution of this linearized equation. Also, we test numerically the invariance condition (3) by considering $s(t;a(m,T),T)$ [cf. Eqs. (2) and (4)] instead of $\mathrm{cn}[4K(m)t/T;m]$. In Sec. IV we numerically investigate the bifurcation behavior at the stability boundaries in the parameter planes m-F and a-F, and lastly, Sec. V concludes the paper.

II. ORDER-CHAOS THRESHOLD

As is well known, MA provides a mathematical criterion to determine approximately the chaotic threshold of a wide variety of dynamical systems. Specifically, MA is concerned

with the occurrence of homoclinic (and heteroclinic) chaos in such systems. Since MA is a first-order perturbative method, we will assume in this section that the dissipation and parametric excitation terms are *weak* perturbations of the underlying integrable system, i.e., $\eta \ll 1$, $\eta F \ll 1$. MA is now considered a standard method, so that we refer the interested reader to the pertinent literature [9–13].

The application of MA to Eq. (1) implies calculating the Melnikov function,

$$M(t_0) = -\eta \int_{-\infty}^{\infty} \{1 + Fp(t+t_0;T)\} \dot{x}_0^2 dt, \qquad (9)$$

associated with either of the homoclinic orbits of the integrable two-well Duffing oscillator:

$$x_0(t) = \pm\sqrt{2}\,\mathrm{sech}(t),$$

$$\dot{x}_0(t) = \mp\sqrt{2}\,\mathrm{sech}(t)\tanh(t). \qquad (10)$$

The Melnikov function (9) measures the distance between the perturbed stable and unstable manifolds in the Poincaré section at t_0. If $M(t_0)$ has a simple zero, then a homoclinic bifurcation occurs, signifying the *possibility* of chaotic behavior. For the sake of clarity, we shall treat separately the effects of the two types of pulse function.

A. Case of the JEF cn

Using the Fourier expansion of cn [3], it is straightforward to recast Eq. (9) with $p(t+t_0;T) \equiv \mathrm{cn}[4K(t+t_0)/T;m]$ into the form

$$M(t_0) = -2\eta \int_{-\infty}^{\infty} \mathrm{sech}^2(\tau)\tanh^2(\tau)d\tau$$

$$-\frac{2\pi\eta F}{\sqrt{m}K} \sum_{n=0}^{\infty} \mathrm{sech}[(n+1/2)\pi K'/K]$$

$$\times \cos[(n+1/2)4\pi t_0/T]$$

$$\times \int_{-\infty}^{\infty} \mathrm{sech}^2(\tau)\tanh^2(\tau)\cos[(n+1/2)4\pi\tau/T]d\tau,$$

$$\qquad (11)$$

with $K'(m) \equiv K(1-m)$ the complementary complete integral of the first kind. The resulting integrals can be evaluated with the aid of standard integral tables [14]. Finally, one obtains

$$M(t_0) = -\frac{8}{3}\eta - 2\pi^2\eta F \sum_{n=0}^{\infty} a_n(m)b_n(T)$$

$$\times \cos[(n+1/2)4\pi t_0/T], \qquad (12)$$

with

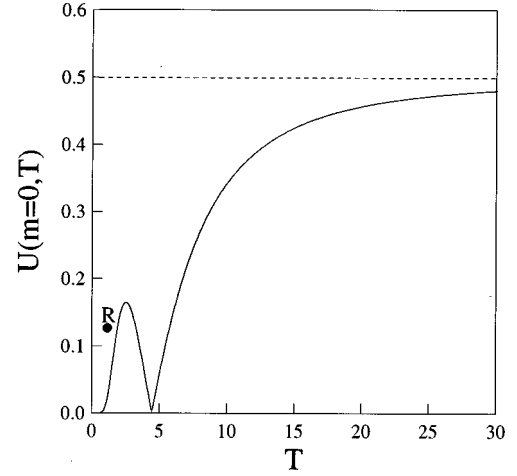$$a_n(m) \equiv \frac{1}{\sqrt{m}K}\mathrm{sech}[(n+1/2)\pi K'/K],$$

FIG. 2. Chaotic threshold function $U(m=0,T)$ for the trigonometric limiting case $(m=0)$ vs period excitation T [cf. Eq. (17)]. $U(m,T)$ is a dimensionless quantity and T is a dimensionless variable.

$$b_n(T) \equiv \{(2n+1)2\pi/3T - [(2n+1)2\pi/T]^3/6\}$$

$$\times \mathrm{csch}[(2n+1)\pi^2/T]. \qquad (13)$$

From Eqs. (12) and (13) one sees that a homoclinic bifurcation is guaranteed for trajectories whose initial conditions are sufficiently close to the separatrix (10) if

$$\frac{1}{F} < U(m,T), \qquad (14)$$

where the chaotic threshold function is

$$U(m,T) \equiv \frac{3\pi^2}{4}\left|\sum_{n=0}^{\infty} a_n(m)b_n(T)\right|. \qquad (15)$$

In order to analyze the behavior in parameter space, consider first the limiting case of a harmonic excitation $(m=0)$. From Eq. (13) one straightforwardly obtains

$$a_n(m=0) = \begin{cases} 1/\pi, & n=0 \\ 0, & n>0. \end{cases} \qquad (16)$$

Therefore,

$$U(m=0,T) = \frac{\pi^2}{2}\left|\frac{1}{T} - \frac{2\pi^2}{T^3}\right|\mathrm{csch}\left(\frac{\pi^2}{T}\right). \qquad (17)$$

A plot of $U(m=0,T)$ is given in Fig. 2. One observes the following features for increasing values of T. First, $U(m=0,T\to0)=0$, i.e., at this limiting value, chaotic motion is not possible since the average of $F\cos(2\pi t/T)$ over any finite time interval tends to 0 as $T\to0$. Second, the threshold function (17) presents a *maximum* at $T=T_{\max} \equiv 2.51...$ of $U(m=0,T=T_{\max}) \simeq 0.1644$, and a *minimum* at $T=T_{\min}(m=0) \equiv \sqrt{2}\pi$ of $U(m=0,T=T_{\min})=0$. Therefore, if one considers fixing the parameter η so as to lie at a regular regime at point R in Fig. 2, then as T is increased, a window of (at least transient) chaos will appear for $0 < T < T_{\min}(m=0)$. This is indeed observed in numerical experiments as can be appreciated in the sequence shown in Fig. 3. Note that for T suf-
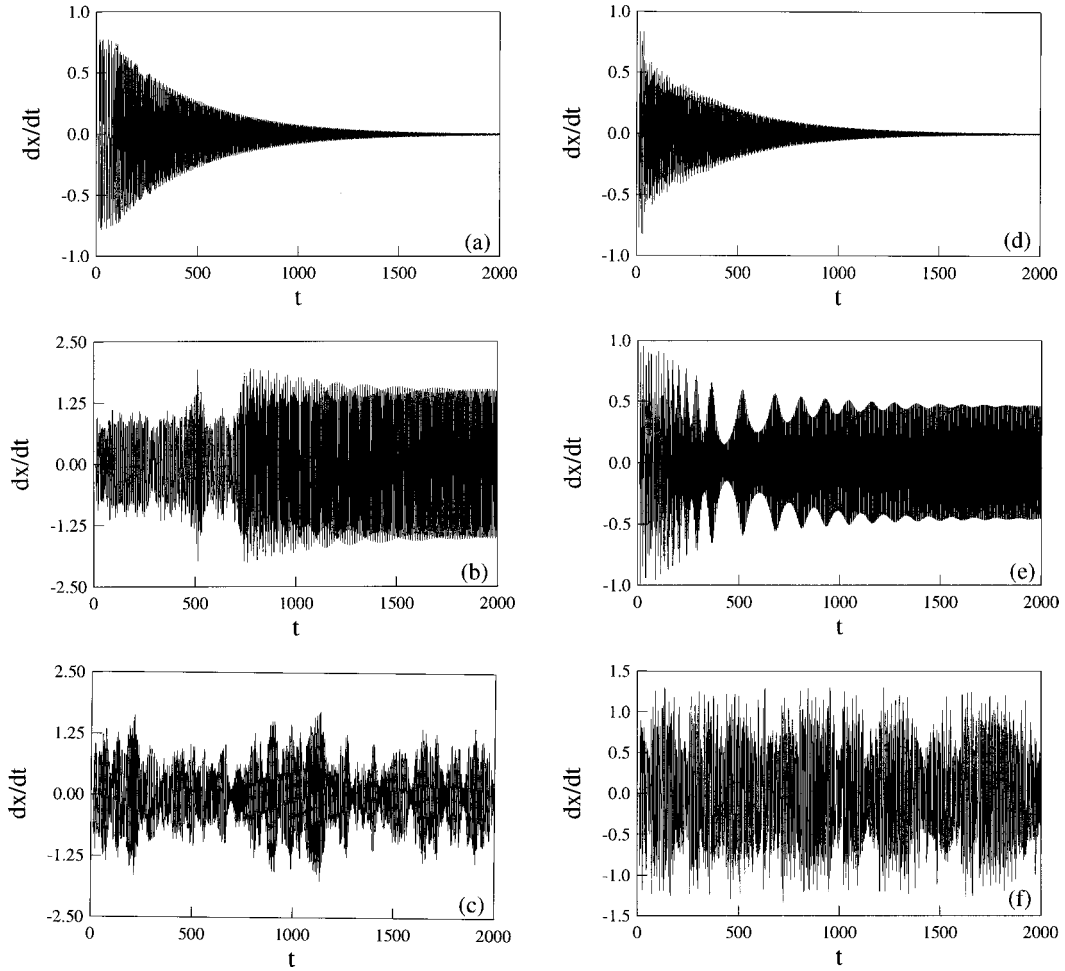
FIG. 3. Velocity time series. The parameters are $\eta=0.005$, $F=100$, $m=0$ (harmonic excitation). (a) $T=1$, (b) $T=1.5$, (c) $T=T_{max}$ $\equiv 2.51...$, (d) $T=3.5$, (e) $T=T_{min}(m=0)\equiv\sqrt{2}\pi$, (f) $T=6.5$. The quantity x is in arbitrary units and t is a dimensionless variable.

ficiently larger than $T_{min}(m=0)$, chaotic behavior is again observed, as expected [cf. Figs. 2 and 3(f)]. Third, for $T>T_{min}(m=0)$ the chaotic threshold function is an increasing function that asymptotically tends to $\frac{1}{2}$ as $T\rightarrow\infty$. In other words, for $F\leq 2$ chaotic behavior is not possible for any period T (see Fig. 2). It is worth mentioning that this result is coherent with that arising from the stability boundary of the solutions ($x=\pm 1$, $\dot{x}=0$) in the T-F plane, namely, that such stability boundary presents its single minimum at $T=T_{min}(m=0)/2$ for which $F=2$ (cf. Ref. [8]). Fourth, at $T=T_{min}(m=0)$, chaotic motion is not expected for any excitation amplitude F, which is a consequence of the 1:1 parametric resonance of the underlying Hamiltonian system. Indeed, as $T_{int}(m)\equiv 2\sqrt{2-m}K(m)$ are the periods of the interior orbits associated with the integrable ($\eta=0$) two-well Duffing equation [cf. Eq. (1)], one finds $T_{min}(m=0)=T_{int}(m=0)$.

Consider now the general case $m\neq 0$. From Eq. (15) one readily obtains

$$U(m,T\rightarrow\infty)=\tfrac{1}{2},$$

$$U(m,T\rightarrow 0)=0. \qquad (18)$$

Figure 4 shows that the qualitative form of the function $U(m=\text{const},T)$ remains the same as that corresponding to the limiting harmonic case. There always exists a T_{min}

$=T_{min}(m)$ such that $U[m,T=T_{min}(m)]=0$, and a $T_{max}\equiv 2.51...,\forall m$ [cf. Eqs. (13) and (15)]. It is worth noting that $T_{min}(m)$ increases from its value at $m=0$ as $m\rightarrow 1$, although the deviation from $T_{min}(m=0)$ is only noticiable for values of m close to 1 (i.e., when the pulses are fairly narrow). This can be appreciated in Fig. 5, where we also plot $T_{int}(m)$ for comparison. While there is a notable deviation after $m\simeq 0.3$, both functions show a monotonously increasing be-
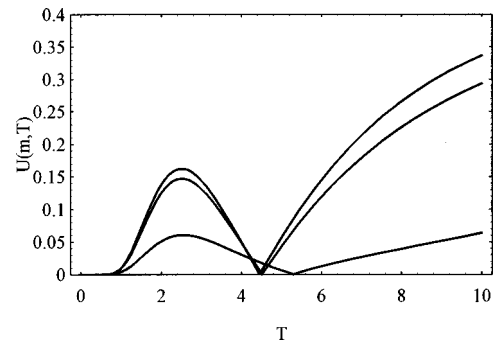

FIG. 4. Chaotic threshold functions $U(m,T)$ vs period T [cf. Eq. (15)] corresponding to different wave forms (values of m) of the excitation. From top to bottom: $m=0.2$, 0.8, and $1-10^{-6}$, respectively. $U(m,T)$ is a dimensionless quantity and T is a dimensionless variable.
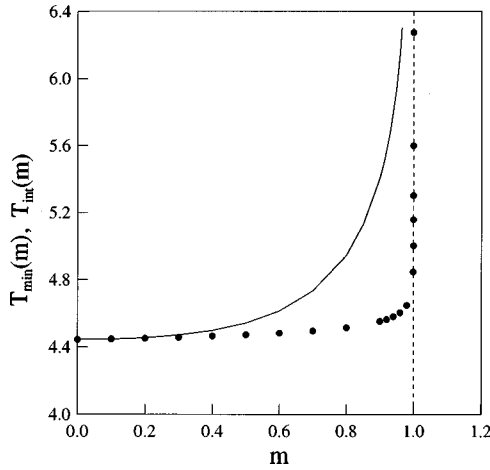
FIG. 5. Plots of functions $T_{\text{int}}(m) \equiv 2\sqrt{2-m}K(m)$ (solid line) and $T_{\min}(m)$ (dots) $[U(m,T_{\min}(m))=0$, cf. Eq. (15)]. $T_{\text{int}}(m)$ and $T_{\min}(m)$ are both dimensionless quantities, and m is a dimensionless variable.

havior, which tends to ∞ as $m \to 1$. Thus, one is tempted to consider the existence of the minima at $T_{\min}(m)$ as an effect of the parametric resonances of the underlying Hamiltonian system. The peak value $U(m,T=T_{\max})$ diminishes from its value at $m=0$ as $m \to 1$, which is coherent with the limit $U(m\to1,T)=0$, i.e., in this limit chaotic behavior is not expected. Now, two remarks are in order. First, with a fixed T around $T_{\max} \equiv 2.51...$, the range of values of the pulse amplitude for which (at least transient) chaotic motion is expected to be observed *decreases* as m is increased. Second, with a fixed $F > 1/U(m,T_{\max})$ [cf. Eq. (14)], the range of values of the period [included in the interval $(0,T_{\min}(m))$] for which (at least transient) chaotic behavior is expected to be detected *increases* as m is increased.

We now study the chaotic threshold as a function of solely the pulse shape parameter m, holding the period constant. Typical plots of the function $U(m,T=\text{const})$ are shown in Figs. 6 and 7. In general, for T sufficiently near a given $T_{\min}(m)$, as in the instance given in Fig. 7, the behavior of the threshold function vs m is qualitatively different from that occurring for values of T sufficiently far from such $T_{\min}(m)$, as in the example depicted in Fig. 6. Figure 7(b) reveals that the dynamics can exhibit *extreme sensitivity* to changes in the pulse wave form, as indeed is illustrated by the sequence of displacement time series displayed in Fig. 8. Note that the chaotic series in Fig. 8(b) corresponds to the value $m=m_{\max}$ at which $U[m,T=T_{\min}(m=0)]$ presents a maximum [Fig. 7(b)] i.e., to the most favorable situation for the onset of chaos.

B. Case of a rectangular-pulse function

Using the Fourier expansion of $s(t;a,T)$ [14], and after evaluating the resulting integrals, we can recast Eq. (9) with $p(t+t_0;T) \equiv s(t+t_0;a,T)$ into the form,

$$M(t_0) = -\frac{8}{3}\eta - 8\eta F \sum_{n=0}^{\infty} c_n(a,T)b_n(T)$$

$$\times \cos[(n+1/2)4\pi t_0/T], \qquad (19)$$

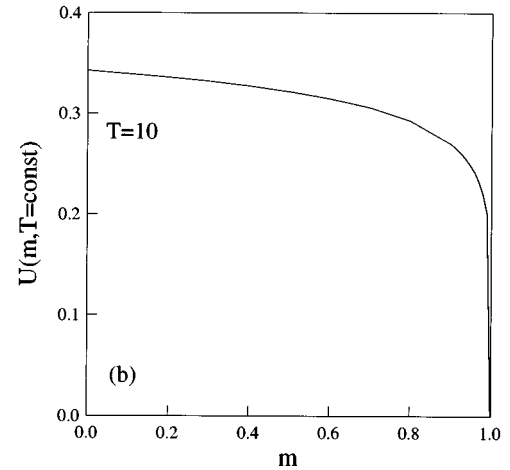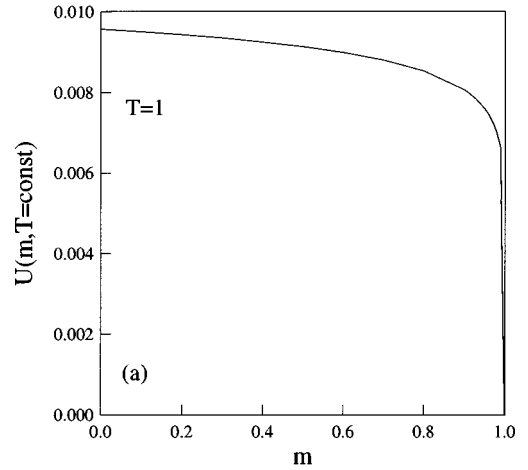

FIG. 6. Chaotic threshold function $U(m,T)$ (dimensionless quantity) vs elliptic parameter m (dimensionless variable) [cf. Eq. (15)] associated with the periods $T=1$ (a) and $T=10$ (b).

with

$$c_n(a,T) \equiv \frac{1}{2n+1}\sin[(n+1/2)2\pi a/T], \qquad (20)$$

and $b_n(T)$ given by Eq. (13). From Eqs. (19) and (20) the necessary condition for the onset of chaos is written

$$\frac{1}{F} < U'(a,T), \qquad (21)$$

where the new chaotic threshold function is

$$U'(a,T) \equiv 3\left|\sum_{n=0}^{\infty} c_n(a,T)b_n(T)\right|. \qquad (22)$$

In order to test the invariance condition (3), we substitute $a(m,T)$ [cf. Eq. (4)] into Eq. (20). Thus, Eq. (22) reduces to the form

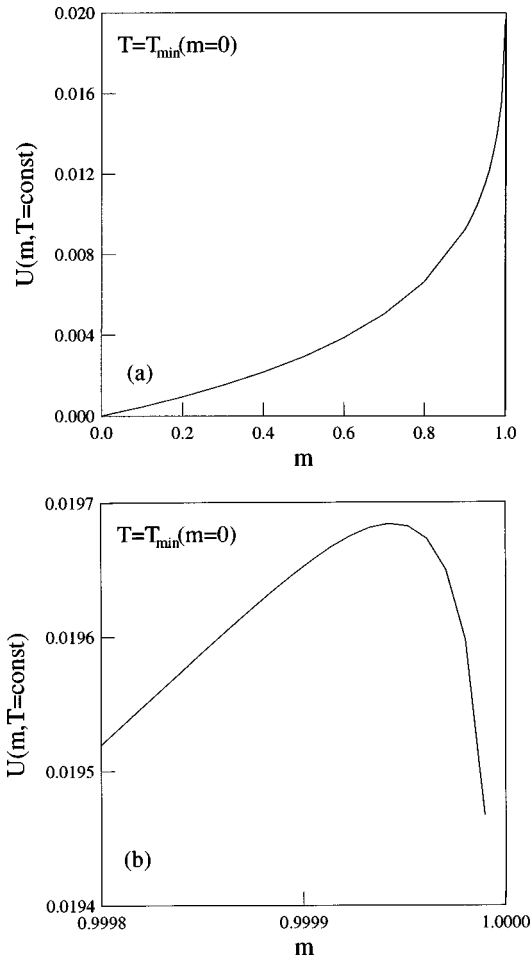$$U'(m,T) \equiv 3\left|\sum_{n=0}^{\infty} c_n(m)b_n(T)\right|, \qquad (23)$$

with

FIG. 7. Chaotic threshold function $U(m,T)$ vs elliptic parameter m [cf. Eq. (15)] for the period $T=T_{min}(m=0)\equiv\sqrt{2}\pi$ (at which chaotic behavior is not possible for a trigonometric excitation) (a), and detail of the maximum region (b). $U(m,T)$ is a dimensionless quantity and m is a dimensionless variable.

$$c_n(m)\equiv\frac{1}{2n+1}\sin\left[\frac{(n+1/2)\pi\arccos\sqrt{1-m}}{\sqrt{m}K(m)}\right]. \quad (24)$$

Figure 9 shows that the form of the function $U'(m=\text{const},T)$ is the same as that of $U(m=\text{const},T)$ (cf. Fig. 4), i.e., there always exists a $T'_{min}=T'_{min}(m)$ such that $U'(m;T'_{min}(m))=0$, and a $T'_{max}=T_{max}\equiv2.51...$, $\forall m$ [cf. Eqs. (13) and (23)]. Also, $T'_{min}(m)$ increases from its value at $m=0$ as $m\rightarrow1$, as $T_{min}(m)$ does. Figure 10 depicts the relative deviation $[T'_{min}(m)-T_{min}(m)]/T_{min}(m)$ showing that it is only noticiable for very narrow pulses (i.e., for values of m very close to 1). This is in agreement with the discussion at the end of the Sec. I: one sees that the invariance condition (3) works better for small than for large periods (cf. Figs. 5 and 10). The function $U'(m,T=\text{const})$ is very similar in shape to $U(m,T=\text{const})$, as can be appreciated in Fig. 11. Figure 12 shows the relative deviation $|U'(m,T=\text{const})-U(m,T=\text{const})|/U(m,T=\text{const})$ vs m for two values of the period. For a fixed period, the deviation drops sharply as the pulses narrow. Again, the deviation is greater for large than for small periods, as predicted. Nonetheless, the range of applicability of condition (3) in the period domain appears to be fairly broad.
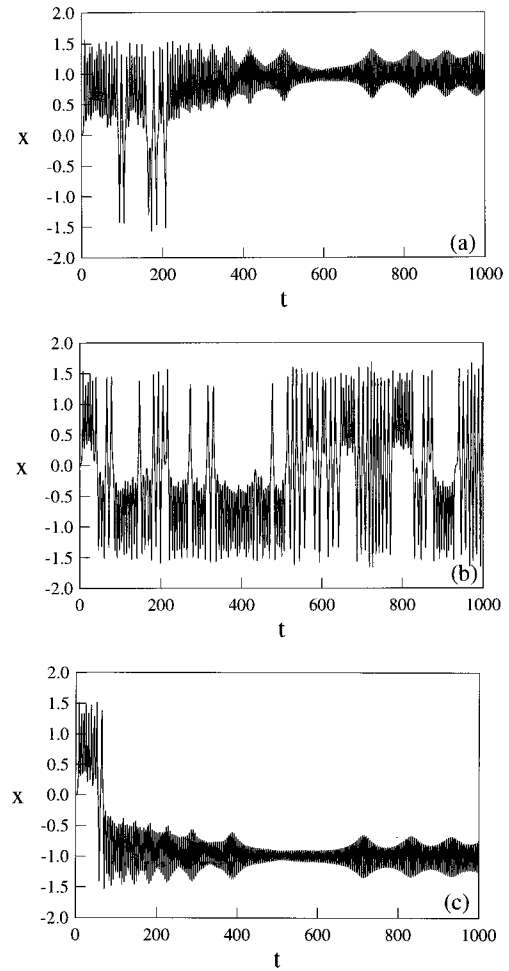

FIG. 8. Displacement time series. The parameters are $\eta=0.005$, $F=170$, $T=T_{min}(m=0)\equiv\sqrt{2}\pi$, (a) $m=0.9998$, (b) $m=m_{max}\simeq0.999\,942\,5$, and (c) $m=0.999\,99$. The quantity x is in arbitrary units and t is a dimensionless variable.

III. STABILITY BOUNDARIES FOR STATIONARY SOLUTIONS

In this section we assume that the driving period T is sufficiently small for the invariance condition (3) to be approximately correct. We can then obtain theoretical estimates of the stability boundaries for the solutions ($x=\pm1$, $\dot{x}=0$), which would be valid for any symmetric-pulse function
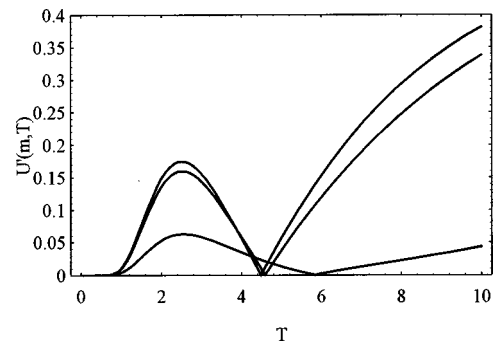

FIG. 9. Chaotic threshold functions $U'(m,T)$ (dimensionless quantity) vs period T (dimensionless variable) [cf. Eq. (23)] corresponding to distinct shapes (values of m) of the pulses. From top to bottom: $m=0.2$, 0.8 and $1-10^{-6}$, respectively.
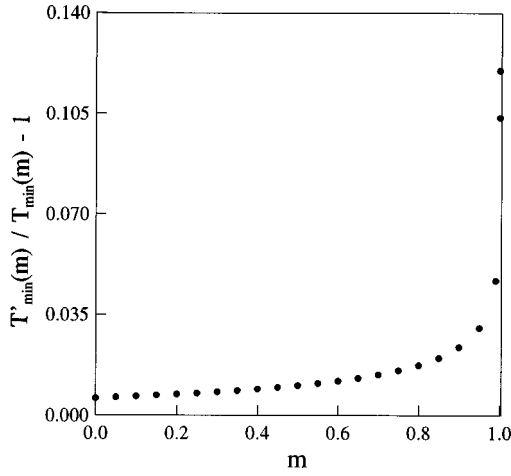
FIG. 10. Relative deviation $[T'_{\min}(m)-T_{\min}(m)]/T_{\min}(m)$ $[U(m,T_{\min}(m))=0, U'(m,T'_{\min}(m))=0$, cf. Eqs. (15) and (23), respectively] vs m (dimensionless variable). The last two plotted points correspond to the values $m=1-10^{-6}$ and $m=1-10^{-15}$, respectively. See Fig. 5 for comparison.

$p(t;T)$. In order to facilitate the comparison with the previously studied harmonic case [8], we shall calculate by using cnoidal pulses. Thus, following Ref. [8] we rewrite Eq. (1) with $p(t;T)\equiv \text{cn}(\omega t;m)$ as

$$\Omega^2 \frac{d^2x}{dt^2}+q[1+2\epsilon \,\text{cn}(2\tau;m)]\frac{dx}{dt}-x+x^3=0, \quad (25)$$
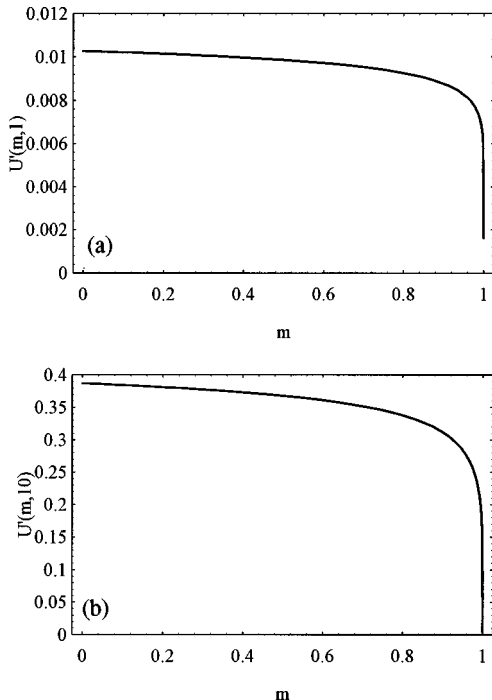
using the transformations

FIG. 11. Chaotic threshold function $U'(m,T)$ (dimensionless quantity) vs elliptic parameter m (dimensionless variable) [cf. Eq. (23)] associated with the periods $T=1$ (a) and $T=10$ (b). Compare with Fig. 6.
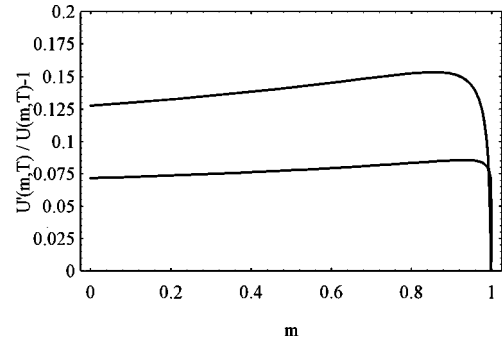

FIG. 12. Relative deviation $|U'(m,T=\text{const})-U(m,T=\text{const})|/U(m,T=\text{const})$ vs m (dimensionless variable) for $T=1$ (bottom curve) and $T=10$.

$$\tau=\frac{1}{2}\,\omega t, \quad \Omega=\frac{\omega}{2}, \quad q=\eta\Omega, \quad \epsilon=\frac{F}{2}. \quad (26)$$

The linearized equation for a perturbation ξ around the pair of stationary solutions $(x=\pm 1, \dot{x}=0)$ reads

$$\Omega^2 \frac{d^2\xi}{dt^2}+q[1+2\epsilon \,\text{cn}(2\tau;m)]\frac{d\xi}{dt}+2\xi=0. \quad (27)$$

We assume that the boundary of stability may be determined from the existence of a periodic solution for ξ. In Ref. [8] the classical Floquet theorem was used to deal with the respective problem corresponding to the limiting harmonic case $(m=0)$. Here we use an elliptic generalization of this procedure, which is based on the existence of generalized Fourier series [15] and on an elliptic harmonic balance method [16]. Thus we may assume the existence of

$$\xi=\frac{A_0}{2}+\sum_{n=0}^{\infty}[A_n \cos(n\varphi)+B_n \sin(n\varphi)], \quad (28)$$

where $\varphi\equiv am(\tau;m)$ is the JEF of parameter m. Since we are here solely interested in a *qualitative* estimate of the stability boundaries in the m-F and T-F parameter planes, we shall limit our treatment to the lowest-order approximation. Thus we truncate the series (28) at $n=1$ and insert the resulting expression into Eq. (27), obtaining

$$\{\Omega^2[(2m-1)\text{cn}(\tau)-2m\text{cn}^3(\tau)]-q\,\text{sn}(\tau)\text{dn}(\tau)$$
$$-2\epsilon q\,\text{sn}(\tau)\text{dn}(\tau)\text{cn}(2\tau)+2\,\text{cn}(\tau)\}A_1$$
$$+\{\Omega^2[2m\,\text{sn}^3(\tau)-(1+m)\text{sn}(\tau)]+q\,\text{cn}(\tau)\text{dn}(\tau)$$
$$+2\epsilon q\,\text{cn}(\tau)\text{dn}(\tau)\text{cn}(2\tau)+2\,\text{sn}(\tau)\}B_1+A_0=0, \quad (29)$$

where we have used $\sin\varphi\equiv\text{sn}(\tau;m)$, $\cos\varphi\equiv\text{cn}(\tau;m)$ [$\text{sn}(\tau;m)$ and $\text{dn}(\tau;m)$ are JEFs of parameter m] and the notation $pq(\tau)\equiv pq(\tau;m)$. From the generalized Fourier series [15] for the above products of JEFs (see the Appendix), if the expansions are limited to the first harmonic, instead of Eq. (29), one has

$$A_0 + 2\epsilon q a_0'(m) B_1 + \left\{ \left[(2-\Omega^2) + \frac{m}{2}\Omega \right] A_1 + q[a_1(m) \right.$$

$$\left. + 2\epsilon a_1'(m)] B_1 \right\} \cos\varphi + \left\{ \left[(2-\Omega^2) + \frac{m}{2}\Omega^2 \right] B_1 \right.$$

$$\left. - q[b_1(m) + 2\epsilon b_1'(m)] A_1 \right\} \sin\varphi$$

$$+ (\text{higher harmonics}) = 0, \tag{30}$$

where $b_1(m)$, $b_1'(m)$, $a_1(m)$, $a_0'(m)$, and $a_1'(m)$ are given in the Appendix by Eqs. (A14)–(A18), respectively. Setting the independent term and the coefficients of $\cos\varphi$ and $\sin\varphi$ to zero, respectively, one gets the equations for A_0, A_1, and B_1. The existence of a nontrivial solution requires the determinant of the respective coefficient matrix to vanish, i.e.,

$$\begin{vmatrix} 2-(1-m/2)\Omega^2 & q[a_1(m)+2\epsilon a_1'(m)] \\ -q[b_1(m)+2\epsilon b_1'(m)] & 2-(1-m/2)\Omega^2 \end{vmatrix} = 0, \tag{31}$$

which gives [cf. Eq. (26)]

$$\epsilon_c(m,T,\eta) = \frac{\alpha_1(m)}{2} \left(1 - \sqrt{1 - \frac{4\alpha_2(m,T,\eta)}{\alpha_1^2(m)}} \right), \tag{32}$$

where

$$\alpha_1(m) \equiv \frac{a_1(m)b_1'(m) + a_1'(m)b_1(m)}{2a_1'(m)b_1'(m)}, \tag{33}$$

$$\alpha_2(m,t,\eta)$$

$$\equiv \frac{a_1(m)b_1(m) + [T/K(m) + (m-2)K(m)/T]^2/\eta^2}{4a_1'(m)b_1'(m)}. \tag{34}$$

Now we make the following remarks. First, for a harmonic excitation ($m=0$), one recovers

$$\epsilon_c(m=0,T,\eta) = \frac{1}{\eta}\sqrt{\eta^2 + \left(\frac{2T}{\pi} - \frac{\pi}{T}\right)^2}, \tag{35}$$

which coincides, as expected, with the result reported in Ref. [8] for the lowest-order approximation. Second, the function $\epsilon_c(m=\text{const},T,\eta=\text{const})$ presents minima at periods $T = \sqrt{2-m}K(m) \equiv T_{\min}(m)/2$, which can be explained as a consequence of the parametric resonances (interior orbits) of the underlying Hamiltonian system [cf. Eqs. (25) and (26)]. Figure 13 shows a comparison between the stability boundary obtained by numerical calculation and first-order perturbation [Eq. (32)] for $\eta=0.2$, $T=T_{\min}(m=0) \equiv \sqrt{2}\pi$. For values of the shape parameter m close to 0, Eq. (32) provides an early estimate. However, the large discrepancies appearing for $m \gtrsim 0.7$ indicate that higher-order approximations are required for narrow pulses. Nonetheless, the first-order approximation qualitatively reproduces the overall form of the stability boundary, in particular, the expected behavior $F \rightarrow \infty$ as $m \rightarrow 1$. The same considerations concerning the limited validity of estimate (32) can be extended to the stability
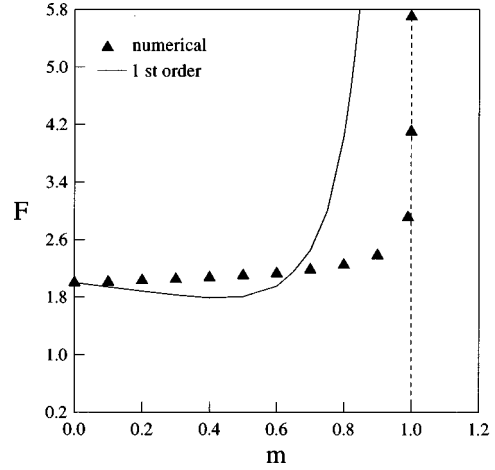

FIG. 13. Stability boundary in the m-F parameter plane (m and F are both dimensionless variables) for $\eta=0.2$, $T=\sqrt{2}\pi$. The results from numerical simulation and from first-order perturbation are shown and compared.

boundaries in the T-F parameter plane. Numerical simulations indeed show that the accuracy of the theoretical estimates diminishes as m approaches 1. As an example, Figs. 14(a) and 14(b) display comparisons between the stability boundary obtained by numerical calculation and first-order perturbation, for $m=0.1$ and $m=0.5$, respectively. In order to test the invariance condition (3), we numerically obtained the stability boundaries corresponding to rectangular-pulse driving (2) for the values $a(m=0.1)$ and $a(m=0.5)$ [according to condition (4)], the remaining parameters being held constant. Figure 15 shows the comparison between such stability boundaries and the respective analytical estimates [from Eq. (32)]. Finally, comparison between Figs. 14 and 15 indicates the utility of condition (3) over the range of periods considered.

IV. BIFURCATION BEHAVIOR AT THE STABILITY BOUNDARIES

Consider first the system (1) subjected to cnoidal pulses. One sees that the stability boundary of the solutions ($x = \pm 1$, $\dot{x}=0$) in the m-F parameter plane is an increasing monotonous function as shown in Fig. 13. The qualitative form of this function remains the same as η and T are varied. The bifurcation behavior is fairly rich along the boundary, i.e., the dynamics appears quite distinct as the parameters m and F are varied to cross different segments of this boundary. This is illustrated by considering two particular types of pathways crossing the boundary: varying the shape parameter m with fixed F, and vice versa. In all the numerical simulations presented in this section we assume $\eta=0.2$. Figure 16 shows the global bifurcation diagram constructed by means of a Poincaré map at $F=3.8$ and $T=2.5183107$. Starting at $m=0$, and taking the transient time as 1000 excitation periods after every increment of $\Delta m=0.01$, we sample 50 excitation periods by picking up the first x value of every excitation cycle. The same initial conditions are set for every new m after Δm is added. Figure 16 shows that in the range $0 \le m < 0.31$ the motion of the system is large-scale cross-well chaos for several m values. Then the system undergoes
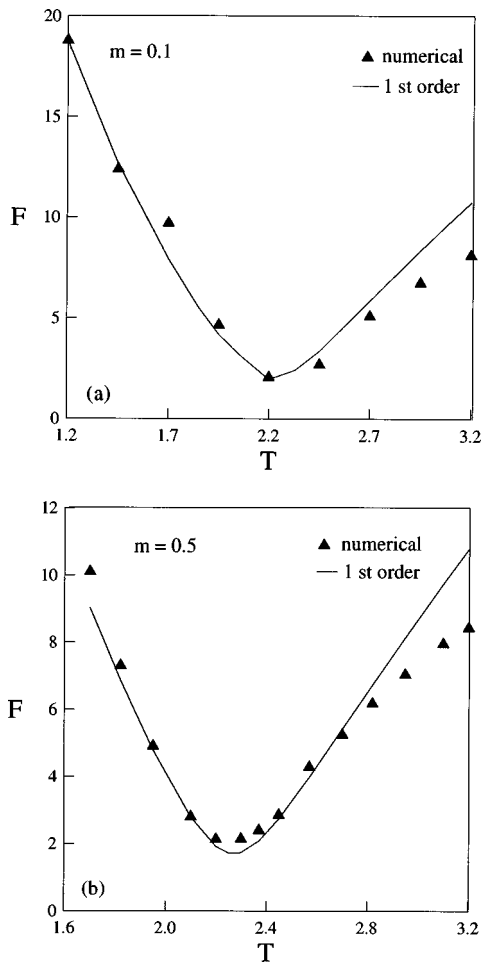
FIG. 14. Stability boundaries in the T-F parameter plane for cnoidal pulses and $\eta = 0.2$: (a) for $m = 0.1$ and (b) for $m = 0.5$, respectively. The results from numerical calculation and from first-order perturbation are shown and compared. T and F are both dimensionless variables.

FIG. 15. Stability boundaries in the T-F parameter plane for a rectangular-pulse function [cf. Eq. (2)] and $\eta = 0.2$: (a) for $a(m = 0.1)$ and (b) for $a(m = 0.5)$, respectively [cf. Eq. (4)]. The results from numerical calculation and from first-order perturbation [cf. Eq. (32)] are shown and compared. T and F are both dimensionless variables.

an inverse interior crisis at $m \cong 0.31$, limiting the chaotic dynamics to inside a smaller region, through the range $0.31 \leqslant m < 0.41$ where phase-locked chaos was detected. From $m = 0.41$ to $m = 1$ the system's overall behavior is inverse period doubling, which is interrupted for a small interval of m, [0.82, 0.84]. In this interval in turn inverse period-doubling cascades take place after an inverse boundary crisis near the beginning of the interval. For $m \in]0.84, 0.99[$, there is the steady behavior of a period-2 attractor, which becomes unstable at $m \cong 0.99$, jumping to the stable stationary solution $(x = 1, \dot{x} = 0)$.

Figure 17 shows a similar bifurcation diagram (x vs F) constructed through a Poincaré map at $m = 0.99$, $T = 2.3271057$, and F ranging from 1 to 10. In this case, the stationary solution ($x = 1$, $\dot{x} = 0$) becomes unstable at $F \simeq 3.1$ and jumps to a single-well period-2 attractor. Period doubling begins at $F \simeq 6.18$ and, after phase-locked chaos appears at $F \simeq 6.67$, the motion becomes large-scale cross-well chaos from $F \simeq 7.03$ (to $F = 10$). One can see that there are very different features of the two routes described above crossing the stability boundary in the m-F parameter plane. In particular, we would emphasize the great richness of the bifurcation behavior as the shape parameter m is varied.
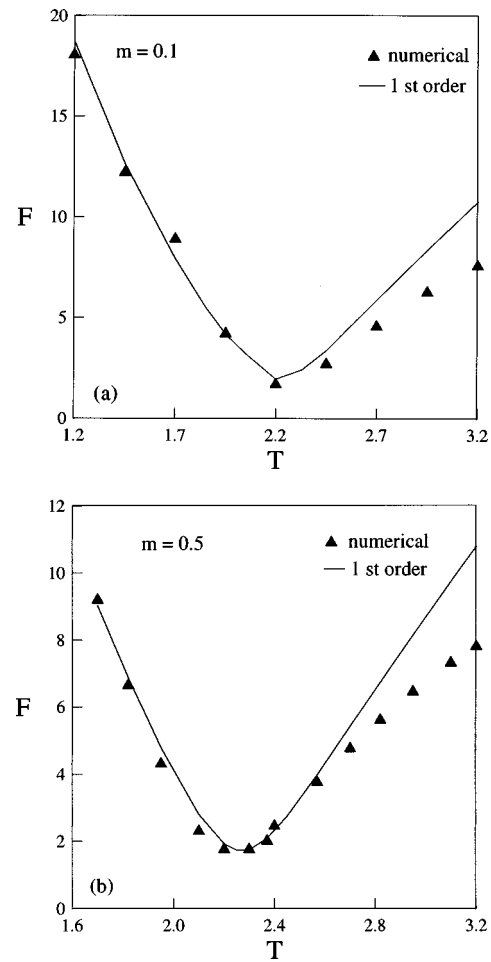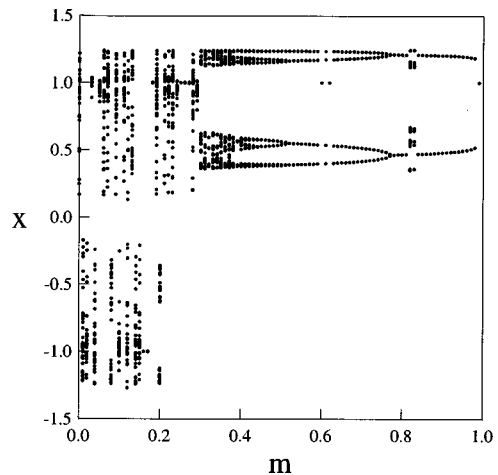

FIG. 16. Bifurcation diagram for the variable x, with $\eta = 0.2$, $F = 3.8$, $T = 2.5183107$, and m (dimensionless variable) in the range $0 \leqslant m \leqslant 1$, corresponding to the system (1) subjected to cnoidal pulses. The quantity x is in arbitrary units.
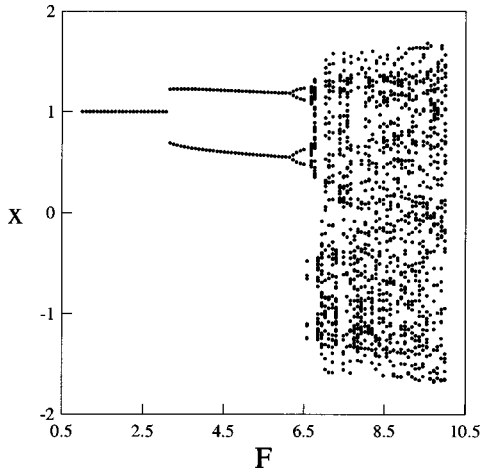
FIG. 17. Bifurcation diagram for the variable x, with $\eta = 0.2$, $T = 2.327\,105\,7$, $m = 0.99$, and F in the range $1 \leqslant F \leqslant 10$ corresponding to system (1) subjected to cnoidal pulses. The quantity x is in arbitrary units and F is a dimensionless variable.

FIG. 18. Bifurcation diagram for the variable x, with $\eta = 0.2$, $F = 3.8$, $T = 2.518\,310\,7$, and a in the range $a(m = 0.999\,999) \leqslant a \leqslant a(m = 0)$ according to condition (4), corresponding to system (1) subjected to rectangular pulses given by Eq. (2). The quantity x is in arbitrary units and a is a dimensionless variable.

Now we consider the system (1) subjected to rectangular pulses given by Eq. (2), in order to test the invariance condition (3). To this end, Fig. 18 shows the global bifurcation diagram x vs a constructed by means of a Poincaré map at $T = 2.518\,310\,7$ and $F = 3.8$. Starting at $a(m = 0, T = 2.518\,310\,7)$ [cf. Eq. (4)], and taking the transient time as 1000 excitation periods after every increment of $\Delta a \equiv a(m, T = 2.518\,310\,7) - a(m + 0.01, T = 2.518\,310\,7)$, we sample 50 excitation periods by picking up the first x value of every excitation cycle. The same initial conditions are set for every new a after Δa is added. Correct comparison between Figs. 16 and 18 must take into account that a is a nonlinear function of m [cf. Eq. (4)]. Nevertheless, one observes that the global bifurcation behavior is rather analogous.

V. CONCLUSION

In this paper we have studied the dynamics of a parametrically damped two-well Duffing oscillator subjected to a periodic string of symmetric pulses, modeled in two different forms: by the JEF cn and by a rectangular-pulse function. We showed that the results remain the same, independently of the specific shape of the pulses, as long as an invariance condition concerning the impulse transmitted by the pulses is imposed. It was shown that, in general, the invariance condition works better for small than for large periods. The following is a summary of the results.

(i) Analytical estimates of the chaotic threshold function were obtained for both types of pulses, and compared under the invariance condition, by means of MA. It was demonstrated that there exist two windows of chaos $[0, T_{\min}(m)[$ and $]T_{\min}(m), \infty[$, for any shape of (either of) the pulses, and this was confirmed by numerical simulations. The impossibility of chaotic motion at the periods $T = T_{\min}(m)$ was explained in terms of parametric resonances of the underlying Hamiltonian system. These results represent well-behaved dynamical properties of the studied system, in the sense that they are insensitive to damping and insensitive to the particular shape of the pulses.
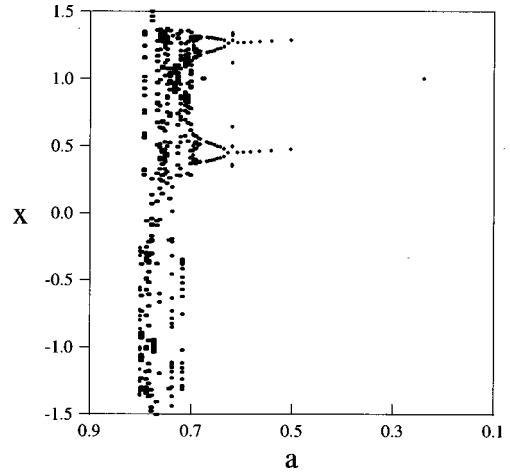
(ii) The stability boundaries of the stationary solutions ($x = \pm 1$, $\dot{x} = 0$) were estimated, to lowest perturbative order, by means of an elliptic harmonic balance method. Numerical calculations indicated that the theoretical curves for the stability boundaries, in the m-F and T-F planes, are reliable for values of m sufficiently close to $m = 0$, and that they remain valid independently of the specific wave form of the pulses.

(iii) The bifurcation behavior along the stability boundary in the parameter planes m-F and $a(m, T)$-F [cf. Eq. (4)] were obtained numerically. It was especially rich in the case where only the shape parameter was varied, holding the remaining parameters fixed.

Finally, we expect that the transmitted impulse invariance condition may be useful for all driven, nonlinear systems whose motions are bounded. Our current work is aimed at exploring this conjecture.

ACKNOWLEDGMENT

APPENDIX: GENERALIZED FOURIER SERIES IN WHICH JACOBIAN ELLIPTIC FUNCTIONS ARE USED

In this appendix it will be shown how to find the expansions of a periodic function $f(\tau)$, with period $4K(m)$, in terms of the periodic set of the so-called *elliptic harmonics* [16],

$$\cos_0(\tau; m) \equiv 1, \quad \cos_n(\tau; m) \equiv \cos(n\varphi),$$

$$\sin_n(\tau; m) \equiv \sin(n\varphi), \tag{A1}$$

where $\varphi = \text{am}(\tau; m)$, $m < 1$ and $n = 1, 2, \dots$ Therefore, one looks for the Fourier coefficients a_n, b_n of

$$f(\tau) = \frac{a_0}{2} + \sum_{n=0}^{\infty} [a_n \cos(n\varphi) + b_n \sin(n\varphi)]. \quad \text{(A2)}$$

They can be obtained by a standard (trigonometric) Fourier expansion of the transformed function $f(\varphi;m)$ in terms of $\cos(n\varphi)$ and $\sin(n\varphi)$:

$$a_n(m) = \frac{1}{\pi} \int_0^{2\pi} f(\varphi;m)\cos(n\varphi)d\varphi, \quad \text{(A3)}$$

$$b_n(m) = \frac{1}{\pi} \int_0^{2\pi} f(\varphi;m)\sin(n\varphi)d\varphi. \quad \text{(A4)}$$

However, instead of changing the function $f(\tau)$ into the form $f(\varphi;m)$ [by using the inverse function $\tau = \text{am}^{-1}(\varphi;m)$], the current procedure uses a set of orthogonal functions defined in the τ variable [the set (A1)]. One, therefore, has

$$f(\tau) = \frac{a_0}{2} + \sum_{n=0}^{\infty} [a_n \cos_n(\tau;m) + b_n \sin_n(\tau;m)], \quad \text{(A5)}$$

where, upon substituting expression (A1) and the formula $d\varphi/d\tau = d[\text{am}(\tau;m)]/d\tau = \text{dn}(\tau;m)$ (cf. Ref. [3]) into the expressions (A3) and (A4), one has

$$a_n(m) = \frac{1}{\pi} \int_0^{4K} f(\tau)\cos_n(\tau;m)\text{dn}(\tau;m)d\tau, \quad \text{(A6)}$$

$$b_n(m) = \frac{1}{\pi} \int_0^{4K} f(\tau)\sin_n(\tau;m)\text{dn}(\tau;m)d\tau. \quad \text{(A7)}$$

Thus, for the products of JEFs appearing in Eq. (29), one straightforwardly obtains

$$\text{cn}^3(\tau;m) = \tfrac{3}{4}\text{cn}(\tau;m) + \cdots, \quad \text{(A8)}$$

$$\text{sn}(\tau;m)\text{dn}(\tau;m) = b_1(m)\text{sn}(\tau;m) + \cdots, \quad \text{(A9)}$$

$$\text{sn}(\tau;m)\text{dn}(\tau;m)\text{cn}(2\tau;m) = b_1'(m)\text{sn}(\tau;m) + \cdots, \quad \text{(A10)}$$

$$\text{sn}^3(\tau;m) = \tfrac{3}{4}\text{sn}(\tau;m) + \cdots, \quad \text{(A11)}$$

$$\text{cn}(\tau;m)\text{dn}(\tau;m) = a_1(m)\text{cn}(\tau;m) + \cdots, \quad \text{(A12)}$$

$$\text{cn}(\tau;m)\text{dn}(\tau;m)\text{cn}(2\tau;m) = a_0'(m) + a_1'(m)\text{cn}(\tau;m) + \cdots, \quad \text{(A13)}$$

where, using Eqs. (A6) and (A7), the coefficients are given by

$$b_1(m) = \frac{1}{\pi} \int_0^{4K} \text{sn}^2(\tau;m)\text{dn}^2(\tau;m)d\tau, \quad \text{(A14)}$$

$$b_1'(m) = \frac{1}{\pi} \int_0^{4K} \text{sn}^2(\tau;m)\text{dn}^2(\tau;m)\text{cn}(2\tau;m)d\tau, \quad \text{(A15)}$$

$$a_1(m) = \frac{1}{\pi} \int_0^{4K} \text{cn}^2(\tau;m)\text{dn}^2(\tau;m)d\tau, \quad \text{(A16)}$$

$$a_0'(m) = \frac{1}{\pi} \int_0^{4K} \text{cn}(\tau;m)\text{dn}^2(\tau;m)\text{cn}(2\tau;m)d\tau, \quad \text{(A17)}$$

$$a_1'(m) = \frac{1}{\pi} \int_0^{4K} \text{cn}^2(\tau;m)\text{dn}^2(\tau;m)\text{cn}(2\tau;m)d\tau. \quad \text{(A18)}$$

Finally, with the aid of standard tables [17], $b_1(m)$ and $a_1(m)$ can be written

$$b_1(m) = \frac{4}{3\pi m}[(2m-1)E(m) + (1-m)K(m)], \quad \text{(A19)}$$

$$a_1(m) = \frac{4}{3\pi m}[(1+m)E(m) - (1-m)K(m)], \quad \text{(A20)}$$

where $E(m)$ is the complete elliptic integral of the second kind.

[1] R. Chacón and J. Díaz Bejarano, Phys. Rev. Lett. **71**, 3103 (1993).

[2] E. A. Jackson, *Perspectives of Nonlinear Dynamics* (Cambridge University Press, Cambridge, 1991), Vol. 1, p. 253.

[3] L. M. Milne-Thomson, in *Handbook of Mathematical Functions*, edited by M. Abramowitz and I. A. Stegun (Dover, New York, 1972), and references therein.

[4] H. J. T. Smith and J. A. Blackburn, Phys. Rev. A **40**, 4708 (1989).

[5] J. A. Blackburn, H. J. T. Smith, and D. E. Edmundson, Phys. Rev. A **45**, 593 (1992).

[6] B. Wu and J. A. Blackburn, Phys. Rev. A **45**, 7030 (1992).

[7] F.-G. Xie and W.-M. Zheng, Phys. Rev. E **49**, 1888 (1994).

[8] F. Xie and G. Hu, Phys. Rev. E **51**, 2773 (1995).

[9] V. K. Melnikov, Trans. Moscow Math. Soc. **12**, 1 (1963).

[10] V. I. Arnold, Sov. Math. Dokl. **5**, 581 (1964).

[11] J. Guckenheimer and P. J. Holmes, *Nonlinear Oscillations, Dynamical Systems, and Bifurcations of Vector Fields* (Springer, New York, 1983).

[12] A. J. Lichtenberg and M. A. Lieberman, *Regular and Stochastic Motion* (Springer, Berlin, 1983).

[13] D. K. Arrowsmith and C. M. Place, *An Introduction to Dynamical Systems* (Cambridge University Press, Cambridge, 1990).

[14] I. Gradshteyn and I. Ryzhik, *Table of Integrals, Series and Products* (Academic, New York, 1994).

[15] J. Díaz Bejarano and A. Martín Sánchez, J. Sound Vib. **134**, 333 (1989); J. Math. Phys. **30**, 1871 (1989).

[16] S. Bravo Yuste, J. Sound Vib. **145**, 381 (1991), and references therein.

[17] P. F. Byrd and M. D. Friedman, *Handbook of Elliptic Integrals for Engineers and Scientists* (Springer-Verlag, Berlin, 1971), p. 303.